FULL PAPER

Development of an Articulated Mobile Robot Moving on Magnetic Curved Walls and Passing Over Obstacles

Shotaro Ueno[a], Mizuki Nakajima[a] and Motoyasu Tanaka[a]

[a]Department of Mechanical Intelligent Systems Engineering, Graduate School of Information Science and Engineering, The University of Electro-Communications, 1-5-1 Chofugaoka, Chofu, Tokyo, Japan

ARTICLE HISTORY
Compiled October 16, 2022

ABSTRACT
We developed an articulated mobile robot that can move on the magnetic curved walls and traverse through obstacles for wall surface inspections of a large tank. This robot is equipped with magnetic wheels and is able to stick to and move on steel wall. We add passive roll joints and turn off the torque of the pitch joints to ensure the wheels keep in contact with the curved surface. The developed robot is tested through experiments in the laboratory and also in a field test at the World Robot Summit 2020. The experiments are conducted to confirm the movements of the robot on the curved wall surface and when the units are lifted for obstacle traversal. As the results, the robot is not able to overcome an obstacle near the wall such as a handrail but is able to move freely on the curved wall surface and traverse some obstacles on the corner.

KEYWORDS
Snake robot; articulated mobile robot; wall climbing; magnet; World Robot Summit 2020

1. Introduction

It is assumed that every few years, large-scale inspections are carried out to detect deterioration of buildings, tanks, and ducts in a plant. During this inspection, plant operations may be necessary to stop. Safety and efficiency are important for detecting corrosion and gas leaks in structures with large surface areas such as tanks. It is expected that the introduction of robots will shorten the operation stop time and make it easier to inspect dangerous areas. For tank inspection on cracks and rust surface, the robot needs to move on the tank wall surface in order to bring the sensors close to the target area. However, it is difficult for the robot to reach the tank because the plant is a complex environment with various structures such as pipes and stairs.

At present, various types of wall-climbing robots are being researched and developed [1,2]. These robots are mainly classified into vacuum adsorption, magnetic adsorption, rotary-wing adsorption, and bionics adsorption.

The vacuum adsorption type [3,4] can move on the wall surface by the adsorption structure and wheels. However, it is difficult to overcome obstacles, and this is one

CONTACT Shotaro Ueno. Email: shotaro.ueno@rc.mce.uec.ac.jp

of the problems to be solved in the future. The two-body negative pressure suction wall-climbing robot [5] is being conducted. This robot uses a two-legged mechanism to overcome obstacles. Also, most of the conventional negative pressure adsorption robots require a cable to connect to an external power source to operate the adsorption device. This greatly limits the range of movement.

Permanent magnet adsorption is very stable. In contrast, because the adsorption is too strong, it also becomes a resistance to the movement of the robot. Magnetic adsorption is limited to magnetic materials, but it has the clear advantage that its adsorption capacity is more stable than other adsorption methods. At present, magnetic adsorption is often used in existing wall-climbing robots [6–12].

Electromagnetic adsorption [13] generates magnetism when the electromagnet is energized, can be adsorbed the robot to the wall, and desorbs when the power is turned off. This solves the problem of obstructing operation by permanent magnets. However, electromagnetic adsorption has drawbacks such as the need for continuous power supply and the heavy electromagnet. At present, electromagnetic adsorption has not been used compared to permanent magnets due to these problems.

Rotary-wing adsorption has the advantages of stable adsorption and less wall roughness requirements. In contrast, this type of robot generally requires a cable to be connected to an external power source. This greatly limits the range of movement. For the above reasons, rotary-wing adsorption wall moving robots are not widely used.

Bionics adsorption [14,15] is a robot made by applying bionics and animals' adsorption methods on walls to the wall-climbing robot. This type of robot has the advantages of small size and wide adaptability. However, this type of robot is not widely used due to its weak load capacity and difficulty in manufacturing adsorption structures.

As for the movement mechanism, the leg type robot has a high ability to traverse obstacles, but the movement speed is low. In contrast, the wheel type and crawler type have high moving speed, but their ability to traverse obstacles is low. It is difficult for them to traverse obstacles located far away from walls. For example, a motorbike type wall-climbing robot [16] can move on curved surfaces and traverse corners. However, this robot needs to move its wheels along the environmental surface, making it difficult to traverse obstacles located far from the wall surface. From the above, it is difficult for conventional wall-climbing robots to achieve both moving speed and obstacle traversal ability. Many of these robots are specialized in wall movement, but cannot move to the wall from the floor or traverse obstacles by themselves.

However, there are various obstacles and narrow spaces in plant facilities. In order to carry out inspection task efficiently, mobility and obstacle traversability are required. Therefore, we focus on an articulated mobile robot that can enter narrow spaces, climb over steps, and climb stairs [17]. In this research, we develop an articulated mobile robot that consists of multiple units and moves on wheels to achieve both mobility and obstacle traversal. There are various structures in the plant facility, and it is expected that cables will hinder the movement of the robot. Many magnetic structures are used in plant facilities such as tanks, walls and ducts. Based on the above, we have adopted an adsorption method that uses permanent magnets that do not require a power source for the adsorption device. In addition, in plant inspection, not only wall movement but also other task such as inspection inside the duct is desired. Since this robot is similar to a general articulated mobile robot, it can also traverse through various environment other than the wall surface.

2. Requirements

Tank wall and in-duct inspections are among the most difficult areas for human inspection at plant facilities. World Robot Summit 2020 Plant Disaster Prevention Challenge, which held in a test field that simulates a typical plant, has been set as the development target. In this competition, there are inspection missions in ducts and on the walls of large tanks. If the robot can adapt to an environment that simulates actual plant inspections, it can contribute to the practical application of robot-assisted plant inspections. In this competition,the total length of the duct is 17 [m], and the internal cross-sectional dimensions are 597 × 397 [mm]. The inspection target is to locate foreign matters and QR markers in the duct. The tank radius is 1.9 [m], height is 5 [m], and it is made of steel. A spiral staircase is installed around the tank. In order to inspect the tank wall surface, it is necessary to move on the curved wall surface and deal with complicated environments such as handrails and steps of the spiral staircase. In particular, the robot must traverse the spiral staircase to reach target inspection areas above the staircase. Therefore, the robot is designed to meet the following requirements in order to realize the tank wall surface inspection.

- Movement on curved wall surface
- Attraction force that does not inhibit wheel lifting
- Friction force to prevent slipping when traversing obstacles
- Equipped with inspection device

In order to move on curved surface of a tank, the robot needs to adapt to the curvature of the wall. However, it is difficult for articulated mobile robots composed of yaw joints and pitch joints[18–23] to keep all wheels in contact with the curved surface due to lack of degrees of freedom. In particular, the smaller the radius of the surface, the more difficult it is to keep contact between the wheels and the curved surface. The goal is to adapt to the tank($R = 1.8$[m]) wall with the smallest radius in the test field. Therefore, the robot in this research adapts to curved surfaces by structure and motion control. The plant has many pipes, which create obstacles in the transition between the wall and the floor and in moving along the wall surface. The three obstacles shown in Figure 15 are difficult for a conventional wall-climbing robot to overcome. In order to overcome these obstacles, it is necessary to lift the magnetic wheels on the floor or the wall. However, if the attraction force of the magnetic wheel is too large, the wheels cannot be lifted. If the friction force of the magnetic wheel is insufficient, the number of contact points decreases when the wheels are lifted on the wall surface, causing slippage. Therefore, these two conditions are expressed in a mathematical formula, and the goal is to develop the magnetic wheel that satisfies the conditions. In addition, the robot needs a manipulator to point sensors at the target when inspecting. We develop simple inspection arms that can be mounted on a curved wall for moving and entering a narrow space. The arm for the tank should be designed to be light enough not to hinder the movement of the curved wall and the traversing of obstacles. The arm for ducts should be small enough to enter into ducts.

3. Design

In this study, we develop an articulated mobile robot(Figure 1) that can move on the curved wall and traverse obstacles to inspect the tank wall surface. Unlike previous articulate mobile robots[18–23] , the developed robot is equipped with magnetic wheels

Table 1. Parameters of MagSnake-1.

Link length [mm]	90
Total size (L×W×H) [mm]	1380×148×120
Wheel radius [mm]	60
Total mass [kg]	8.1
Max moving speed [m/s]	0.20

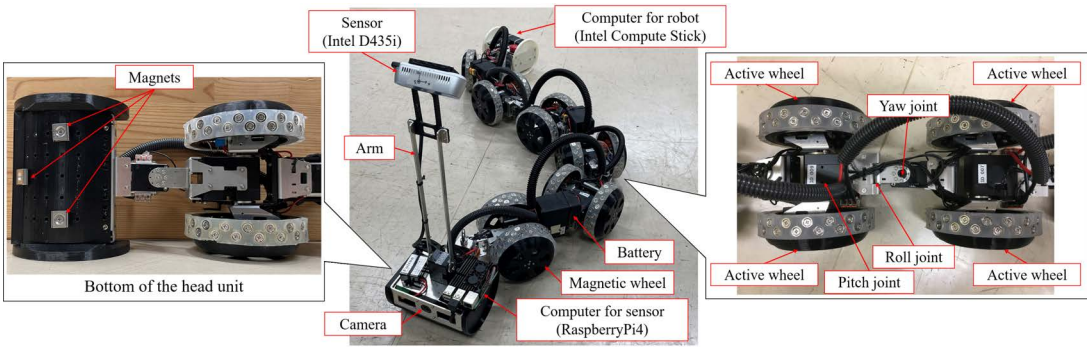

Figure 1. Structure of the robot.

and passive roll joints. The magnetic wheel is a mechanism for adsorbing to wall and moving on the wall surface. The passive roll joint is a mechanism for keeping contact between wheels and the curved surface. The developed robot is shown in Figure 1, and the specifications are shown in Table 1. The structure of the robot is divided into several units as shown in Figure 2. There are three types of units: body unit, head unit, and tail unit. Body unit is a unit that constitutes the main body of the robot and has active magnetic wheels. Head unit is a unit equipped with a fisheye camera, a sensor arm for inspection, and a computer for sensor control. Tail unit is a unit equipped with a fisheye camera, a computer for controlling motors, a battery, and an emergency stop button. Head unit and tail unit are equipped non-magnetic dummy wheel so that they can be steered easily. However, a few magnets are installed at the bottom of the head unit so that attraction forces for maintaining the posture can be obtained.

This section describes passive roll joints related to curved surface adaptation, magnetic wheels related to sticking to the wall and obstacle traversal, and arms related to inspection functions.

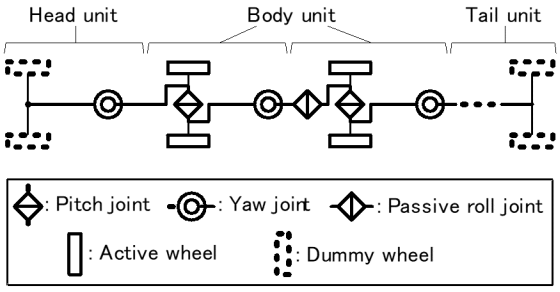

Figure 2. Model of the robot.

3.1. Passive roll joint

In order for the robot to move on the wall surface while generating sufficient attraction force, it is desirable to move while keeping as many wheels in contact with the tank wall surface as possible. When an articulated mobile robot travels on a plane, the contacts between the wheels and the plane are maintained. However, when traveling on a curved surface, the contacts between the wheels and the plane is not guaranteed. Even if the wheels are made compliant, the multi-linkage type robot cannot keep contact between all wheels due to accumulated errors.

In order to maintain the contacts between the curved surface and the wheels, passive roll joints are added between the body unit of the robot. The pitch joints are also passively rotated by turning off the torque. With the attraction force from the magnetic wheels, the passive roll joints and pitch joints are passively orientated to cope with the curved surface of the wall.

In addition, the rotational range of the passive roll joint is determined so that unit lifting motion is not adversely affected. Here, the required range of motion of the roll joints is obtained numerically with a model of two units (Figure 3). A model with the yaw joint angle ϕ is placed with the rear wheels in contact with the curved surface at the orientation of the unit θ. The combination of the pitch joint angle and roll joint angle at which the front wheels almost contact the curved surface when θ and ϕ are changed is obtained from the geometric relationship. However, contact is assumed to occur when the minimum distance between the wheel and the curved surface becomes minute, and point contact between the wheel and the curved surface is a condition for contact. The range of motion of the yaw joint is mechanically limited to ± 60[deg]. The results for yaw joint angles $\phi = 0, 45, 60$[deg] are shown in Figure 4. When the orientation of the unit on the curved surface is $\theta = \pm 45, \pm 135$[deg] and the yaw joint angle is $\phi = 0$[deg](Figure 3), the required roll joint angle is the largest. By referring to the parameter of the tank to be inspected, the maximum required roll joint angle is ± 2.6[deg]. Therefore, the rotational range of the developed robot is set to ± 3[deg] with a margin. The structure of the passive roll joint on the developed robot is shown in Figure 5. The passive roll joint is mainly composed of base frame, yaw frame and stopper. The base frame is fixed to the motor of the pitch joint. The yaw frame is fixed to the servo horn of the yaw joint. The base frame and yaw frame are connected by a roll axis and rotate passively. The stopper is fixed to the base frame and limits the rotational range of the passive roll joint. Furthermore, the stopper receives the load in the thrust direction generated at the passive roll joint. The two body units connected by the passive roll joint are in the state shown in Figure 6a when the passive roll joint rotates. Figure 6b shows the robot that adapts to curved surface with the passive roll joints. By rotating passively the pitch joints and roll joints, all magnetic wheels are in contact with the curved surface ($R = 1.8$)[m] (Figure 6b).

3.2. Magnetic wheel

3.2.1. Structure

In previous researches, several wall climbing methods have been considered such as adhesive[24], negative pressure[25,26] and magnetic[27]. In the adhesive method, the adhesive strength will be reduced over time due to dust or deterioration of the material. The method that uses negative pressure is not suitable for curved surfaces or obstacle traversing because the suction unit must be in contact with the wall without any

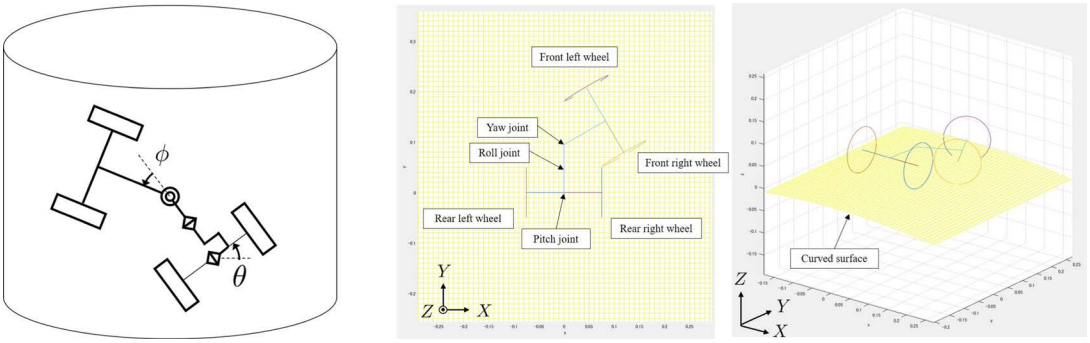

Figure 3. Orientation of the unit on curved surfaces θ and yaw joint angle ϕ.

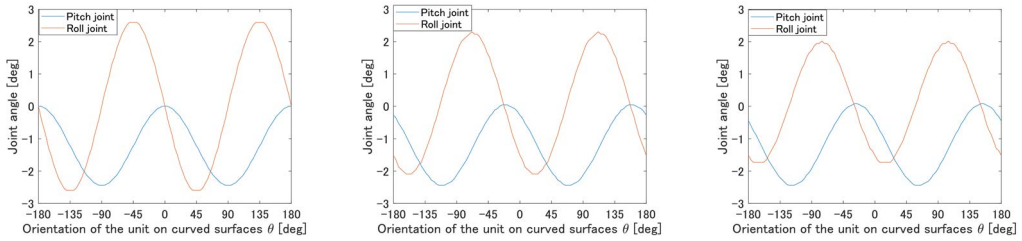

(a) $\phi = 0$[deg]. (b) $\phi = 45$[deg]. (c) $\phi = 60$[deg].

Figure 4. Roll joint angle and pitch joint angle where the wheels and curved surface contact.

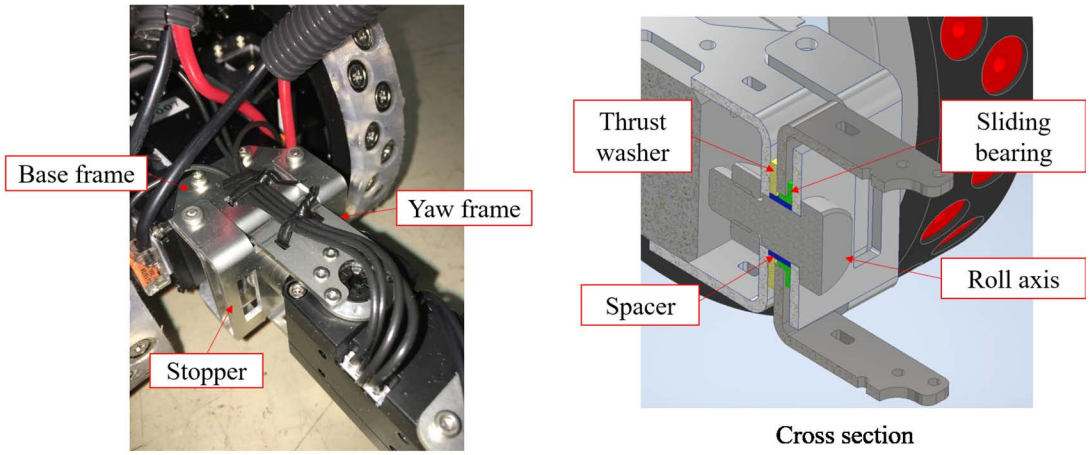

Figure 5. Structure of the passive roll joint.

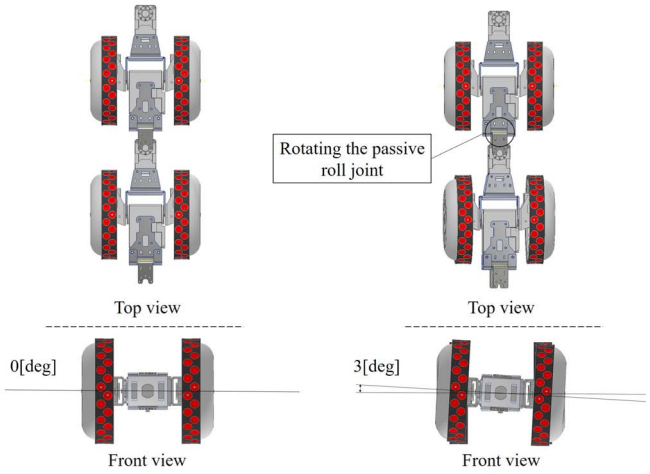

(a) CAD model of the body units when the passive roll joint is 0[deg] and 3[deg].

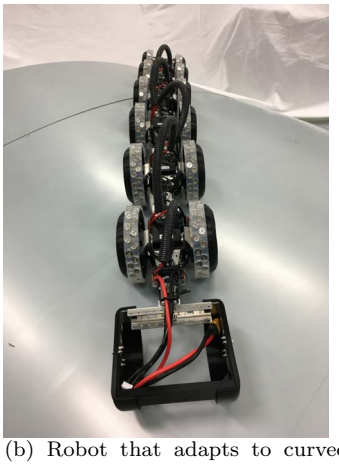

(b) Robot that adapts to curved surface (R=1.8) with the passive roll joints.

Figure 6. The movement of passive roll joint.

clearance. Since the target inspection tank is magnetic, a method using magnetic force is adopted. Permanent magnets are used as the adsorption mechanism to reduce the weight and simplify the system. Neodymium magnets are used because of their light weight and strong attraction force.

The relationship between the magnitude of the magnetic force and the distance between the magnetic poles is important for the position of the magnet. The magnetic force, which is the force acting between the magnetic poles, is expressed by Coulomb's law of magnetic force as follows.

$$F = k_m \frac{m_1 m_2}{r^2} \tag{1}$$

The magnitude of the magnetic force is proportional to product of the respective magnetic quantities m_1[Wb] and m_2[Wb], and inversely proportional to square of the distance r[m] between the poles where, k_m is a proportionality constant. In order to generate magnetic force effectively for wall climbing, it is preferable to place magnets in contact with the wall. Therefore, magnetic wheels (Figure 7) with magnets placed around the periphery of the wheels are developed. The wheel is formed with PLA materials by using a 3D printer, and the tire is molded with silicone rubber KE-1310ST (Shin-Etsu Chemical Co., Ltd.). A ring-shaped magnets are fixed to the wheel with non-magnetic screws. A rubber O-ring is inserted between the ring-shaped magnet and the wheel to adjust the fixed position of the magnet. In addition, the motor is placed inside the wheel to reduce the width of the robot. The wheel diameter is kept as small as possible within the range where the motor can be stored inside. The number of magnets is the number of magnets lined up without interruption around the circumference of the wheel.

The attraction force and the friction force of the magnetic wheel can be adjusted by changing the distance δ between the magnet and the tire surface. The friction and attraction forces are measured when the distance δ between the magnet and the tire surface is changed using the created magnetic wheel. Attraction force is measured by pulling upward a magnetic wheel adsorbed on a steel plate placed horizontally

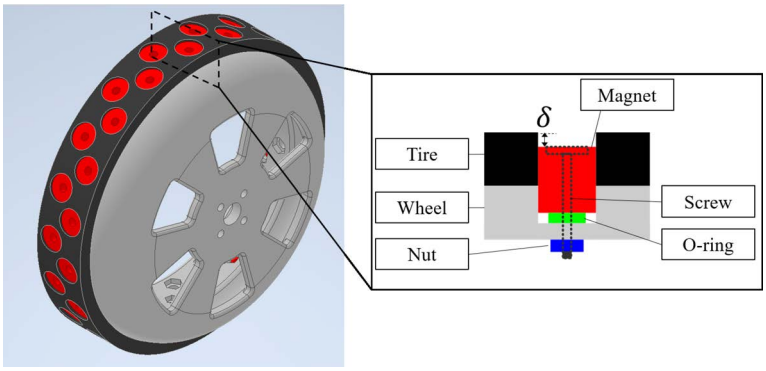

Figure 7. Magnetic wheel.

(Figure 8a). Friction force is measured by pulling two magnetic wheels adsorbed on a steel plate placed horizontally sideways (Figure 8b). To prevent the wheels from rolling, the two magnetic wheels are connected by a component and measured. The measured value divided by two is the friction force per magnetic wheel. A digital force gauge FGJN-5 (NIDEC-SHIMPO Co.) is used for the measurement. A steel plate with a thickness of 6[mm] is used as the magnetic material. Ten measurements are taken at each distance. The measured results of the attraction force and friction force of the magnetic wheel according to the distance δ are shown in Figure 9. The standard deviations of the measured values for all wheels (δ=1.5mm) are 0.73[N] for the attraction force and 0.21[N] for the friction force. The attraction force decreases as the distance δ increased. The friction force has a quadratic relationship and has the highest value around distance δ =1-1.5[mm]. By adjusting the distance δ based on the measurement results, the attraction force and friction force can be adjusted depend to the requirements.

3.2.2. Attraction force

When traversing obstacles or discontinuous surfaces, it is necessary to lift the unit by stripping the magnetic wheel from the wall or floor surface. In particular, a large pitch joint torque is required to lift the unit from a flat surface against the attraction force. As shown in Figure 10a, the attraction force of two wheels $2F_a$ is generated at the contact point between magnetic wheels and surface, and the gravity $M_l g$ is generated at the center of gravity of the lifting part. Let the mass to be lifted be M_l, the acceleration of gravity be g, and the distance between the pitch joint and the contact point be l, and the distance between the pitch joint and the center of gravity be l_{cm}. The moment around the pitch joint is $2F_a l$ due to the attraction force and $M_l g l_{cm}$ due to gravity. To lift the lifting part up, the required pitch joint torque must exceed the moment caused by the gravitational and the attraction force of magnetic wheels. Therefore, the condition of τ is set as follows.

$$\tau > M_l g l_{cm} + 2F_a l \tag{2}$$

From the equation above, the attraction force per magnetic wheel that can be lifted is set as follows.

$$F_a < \frac{\tau - M_l g l_{cm}}{2l} \tag{3}$$

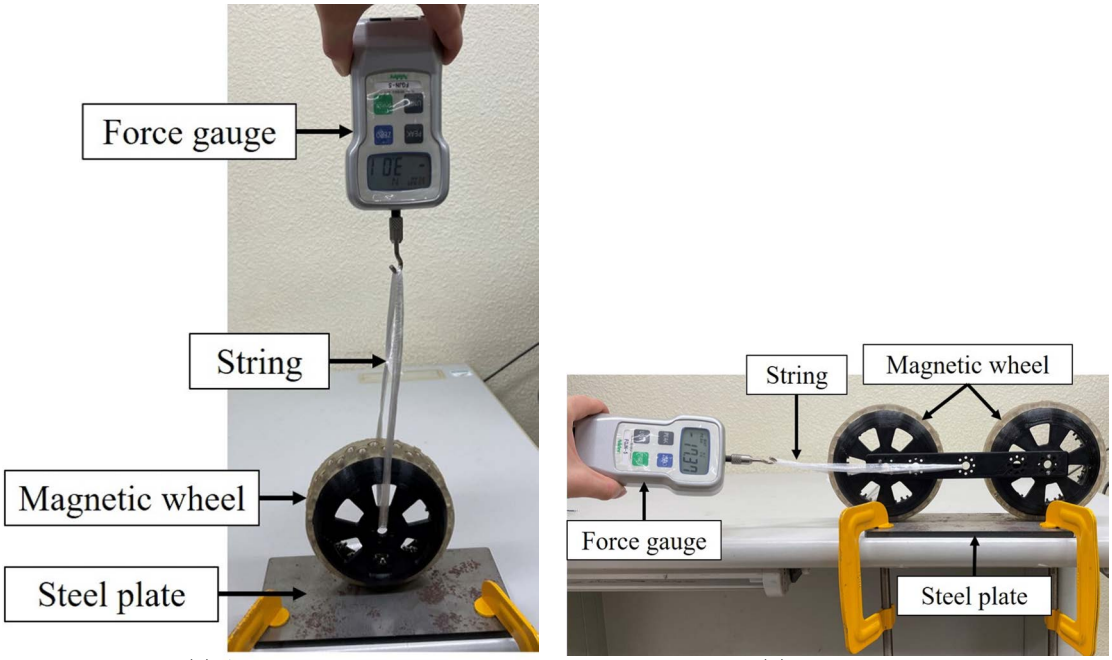

(a) Attraction force. (b) Friction force.

Figure 8. Measurement of force.

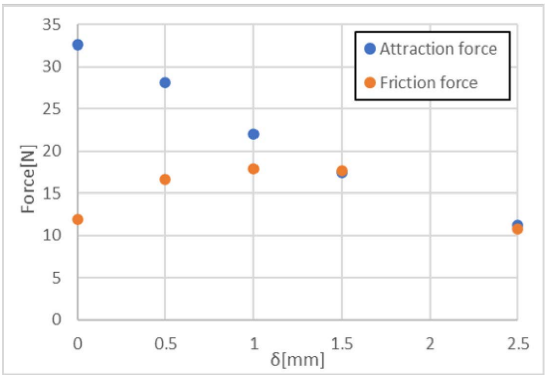

Figure 9. Relation between attraction/friction and distance δ.

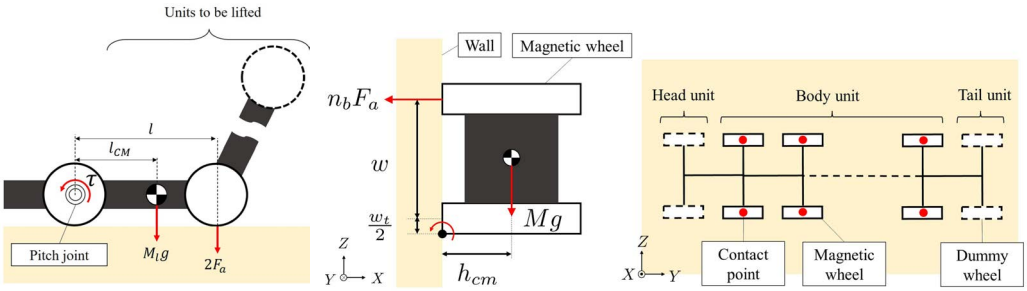

(a) Lifting the unit. (b) Moving horizontally.

Figure 10. Attraction force acting on the robot.

The robot is more likely to peel off from the wall when it moves horizontally on the wall because the distance between the vertical contact points is the smallest as shown in Figure 10b. Let the mass of the robot be M, the height of the center of gravity be h_{cm}, the distance between the magnetic wheels be w, the width of the tire be w_t, the number of body units be n_b, and the acceleration of gravity be g. The attraction force of wheels $n_b F_a$ is generated at the contact point between magnetic wheels and surface, and the gravity Mg is generated at the center of gravity. The moment around the edge of the lower magnetic wheel is $n_b F_a \left(w + \frac{w_t}{2}\right)$due to the attraction force and Mgh_{cm} due to gravity. Therefore, the condition that the robot does not peel off from the wall is set as follows.

$$n_b F_a \left(w + \frac{w_t}{2}\right) > Mgh_{cm} \tag{4}$$

The attraction force per magnetic wheel F_a can be obtained as

$$F_a > \frac{Mgh_{cm}}{n_b \left(w + \frac{w_t}{2}\right)}. \tag{5}$$

However, this is a conditional expression that indicates the upper and lower limit of the attraction force and is independent from the friction force. By substituting the parameters in Table 2 into the above equation, the condition for the attraction force is 7.4[N]$< F_a <$ 18.4[N].

3.2.3. Friction force

When the robot is climbing on a vertical surface, the friction force of the magnetic wheel must exceed its own weight to prevent from sliding down. Since the friction force is generated at the contact points between the magnetic wheel and wall, it varies depending on the number of these contact points. In particular, when the robot is traversing an obstacle on a wall(Figure 11), the number of contact points is greatly reduced and the friction force is decreased. In this case, the robot must keep enough contact points to generate sufficient friction force. Let the mass of the robot be M, the friction force per magnetic wheel be F_f, the number of body units be n_b, and the acceleration of gravity be g. When the body unit mass is M_b, the head unit mass is M_h, and the tail unit mass is M_t, the robot mass is $M = M_b n_b + M_h + M_t$. Since there are two magnetic wheels in one body unit, the friction force generated per unit is $2F_f$. Let the number of body units to be lifted be n_l, the friction force on the robot

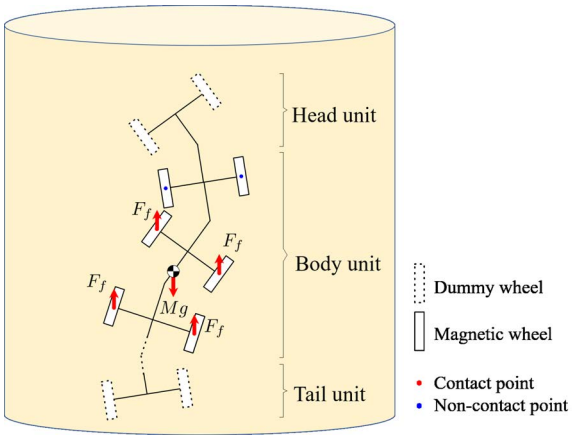

Figure 11. Friction force acting on the robot.

Table 2. Calculation parameters.

M_h[kg]	0.278
M_b[kg]	1.171
M_t[kg]	0.794
M_l[kg]	$M_h + M_b$
n_b	6
n_l	2
l[mm]	180
w[mm]	97
w_t[mm]	21
l_{cm}[mm]	140
h_{cm}[mm]	60
h[mm]	44
τ[Nm]	8.6
g[m/s^2]	9.81

is $2F_f(n_b - n_l)$. Therefore, when n_l of body units are lifted, the condition to prevent the robot from sliding is set as follow.

$$2F_f(n_b - n_l) > (M_b n_b + M_h + M_t)g \tag{6}$$

The friction force per magnetic wheel F_f can be obtained as

$$F_f > \frac{(M_b n_b + M_h + M_t)g}{2(n_b - n_l)}. \tag{7}$$

This is a conditional expression that indicates the lower limit of frictional force. By substituting the parameters in Table 2 into the above equation, the lower limit of friction force is 9.93[N]. From the equation (3)(5)(7) and Figure 9, the distance $\delta =$ 1.5[mm] is determined to be the appropriate attraction and friction force.

Table 3. Parameters of the arm.

	Arm for tank inspection	Arm for duct inspection
Length[mm]	380	227
Weight[kg]	0.200	0.327

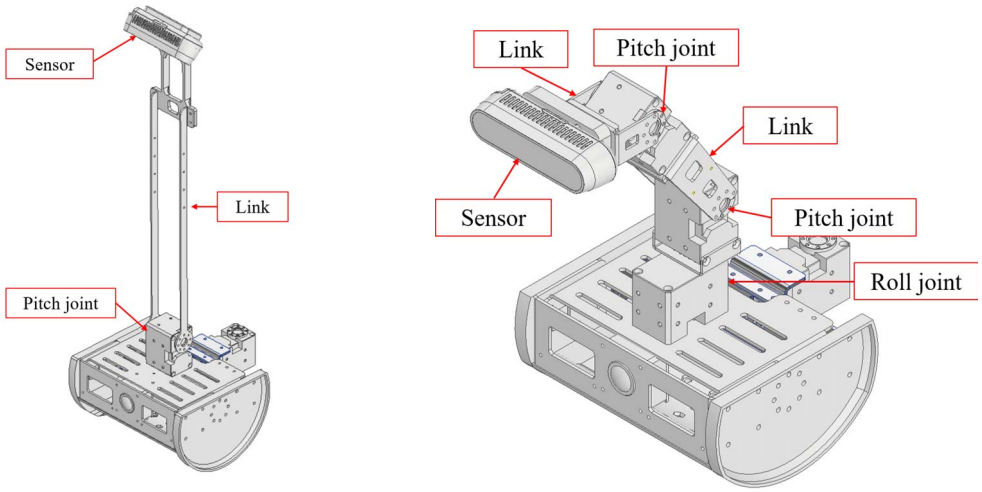

(a) Arm for tank inspection.

(b) Arm for duct inspection.

Figure 12. Structure of the arm.

3.3. Arm

Two types of arms are designed for tank inspection and duct inspection respectively, as shown in Figure 12 . The arm for inspecting the tank wall is designed to be lightweight to reduce the risk of falling from the wall. The arm length is designed long enough to keep the inspection target within the viewing angle of the sensor. From the equation (3)(5)(7), the condition for the attraction force is 7.6[N]$< F_a <$ 17.6[N] and the lower limit of the friction force is 10.2[N] when this arm is mounted. Figure 9 shows that the weight of the arm satisfies the conditions at $\delta = 1.5$[mm]. The arm for duct inspection is designed small enough to be operated in a narrow space. The maximum height of the robot equipped with this arm is 298[mm], which is large enough to enter the duct, compared to the height of 397[mm] inside the duct. The specifications of each arm are shown in Table 3. Both arm are equipped with an Intel D435i as a sensor for inspection. Each joint is driven by a ROBOTIS servo motor. The links are made of aluminum and PLA materials. The arm for the tank inspection has 1 degree of freedom, and the arm for the duct inspection has 3 degrees of freedom.

4. Control

This robot changes its motion control according to its environment. It has two types of control: 3-D steering control for moving on a plane or a curved surface, and Obstacle traversal control for changing the moving surface and overcoming obstacles.

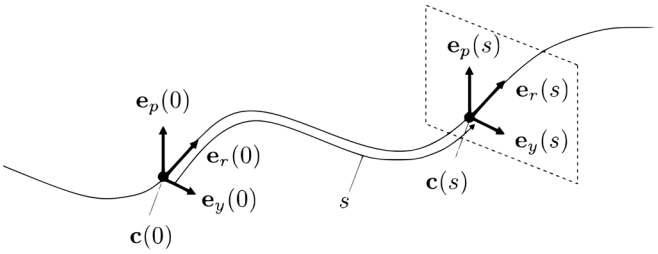

Figure 13. Definition of a continuous backbone curve.

4.1. 3-D steering control

This robot is operated by a shift control [28]. The continuous curve model in 3D space is represented using the backbone coordinate system $\mathbf{e}_r, \mathbf{e}_p, \mathbf{e}_y$ as shown in Figure 13.

$$\begin{cases} \frac{d\mathbf{c}(s)}{ds} & = \mathbf{e}_r(s) \\ \frac{d\mathbf{e}_r(s)}{ds} & = \kappa_y(s)\mathbf{e}_p(s) - \kappa_p(s)\mathbf{e}_y(s) \\ \frac{d\mathbf{e}_p(s)}{ds} & = -\kappa_y(s)\mathbf{e}_r(s) \\ \frac{d\mathbf{e}_y(s)}{ds} & = \kappa_p(s)\mathbf{e}_r(s) \end{cases} \tag{8}$$

where $\mathbf{c} = [x(s), y(s), z(s)]^T$ is a vector representing the coordinates of a continuous curve, and s is the length variable along the curve. $\kappa_p(s), \kappa_y(s)$ are the curvature around the pitch and yaw axes. These parameters of curvature are determined by the operator. i-th yaw joint angle ϕ_i and pitch joint angle ψ_i are given by integrating $\kappa_p(s), \kappa_y(s)$ in the vicinity of each joint.

$$\begin{aligned} \phi_i &= -\int_{s_h-2il}^{s_h-2(i-1)l} \kappa_y(s)ds \\ \psi_i &= -\int_{s_h-(2i+1)l}^{s_h-(2i-1)l} \kappa_p(s)ds \end{aligned} \tag{9}$$

s_h is the leading position of the robot on the curve. By changing the value s_h, the range of the robot body on the curve changes, and a Follow-the-Leader control is performed along the continuous curve. However, this robot needs to adapt to the curved surface by acting passively. Therefore, the torque of the pitch joints are turned off and only the target angle of the yaw joints is used. By passively rotating the roll and pitch joints, the robot can keep contact with the curved surface. Only the first pitch joint is controlled to keep posture of the head unit. In addition, the rotating speed of the wheels are controlled by considering the curvature of the continuous curve and the offset position of the wheels[17].

The continuous curve for the developed robot is designed as shown in Figure 14. The joint angles are calculated based on the Follow-the-Leader control. The torque of the pitch joints are turned off and the robot can adapt to the curve surface of the tank wall as shown in Figure 14c. In Figure 14b, the pitch joints colored in purple indicate that they are controlled passively.

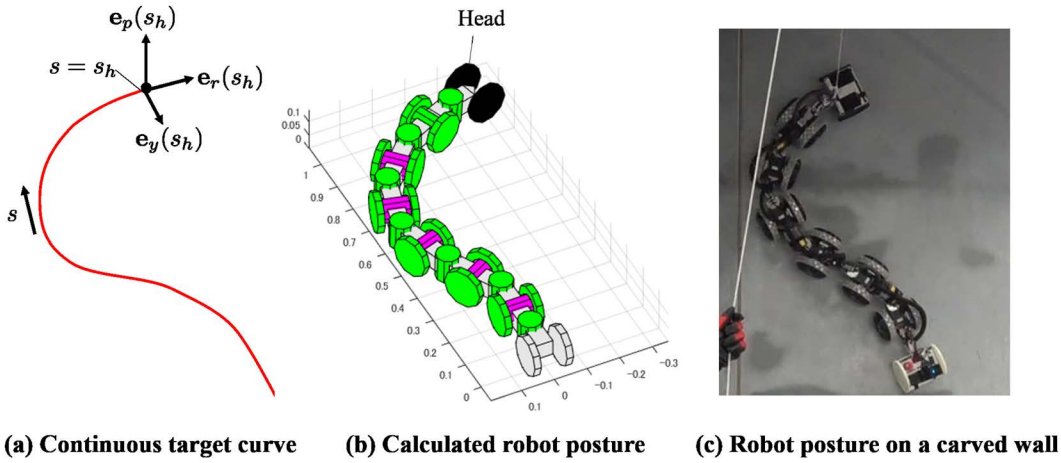

Figure 14. Continuous target curve and robot posture.

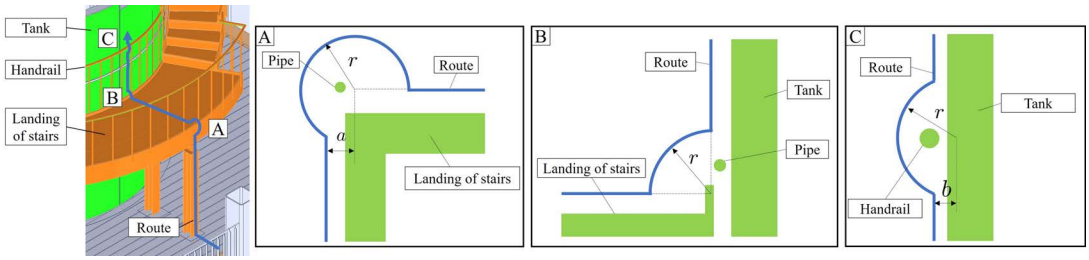

Figure 15. Assumed obstacles and traversal routes. $r = 0.13$[m], $a = 0.08$[m], $b = 0.05$[m].

4.2. Obstacle traversal control

The pitch joints must be activated to lift the unit to traverse obstacles. However, if all the pitch joints are activated, the robot cannot adapt to curved surface. Therefore, the robot can traverse obstacles by controlling the pitch joints partially. Figure 15 shows the path taken by the robot to reach the upper side of the tank wall. There 3 types of obstacles on the route: a 270[deg] corner when moving from the pillar to the landing of the staircase(A), a 90[deg] corner when moving from the landing of the staircase to the wall(B), and a handrail near the wall(C). In this study, we propose an obstacle traversal control by designing a moving route to traverse each of these obstacles, as shown in Figure 15. Obstacle traversing routes are designed for each obstacle. Each obstacle traversing route consists of of straight lines and circular arcs. Two body units of this robot are lifted on the wall to traverse obstacle C. The arc length of the route at obstacle C is designed so that the number of body units to be lifted is 2 or less. The routes of obstacle A and B are shaped like connecting two vertical straight lines with an arc in order to avoid a small pipe and cross the corner. In the route of obstacle A, the center of the arc is shifted toward the wall so that the lifted unit is not too far from the wall. The pitch joint angles are geometrically calculated so that the pitch axis follows these routes. All yaw joints are set to be 0[deg] in this control. The wheel velocity is calculated from the distance traveled by the pitch axis.

The range in which the pitch joints are activated is set according to each obstacle traversal route. In the following, we explain the posture when the robot traversing a handrail, which is particularly prone to peeling. As shown in Figure 16, on the

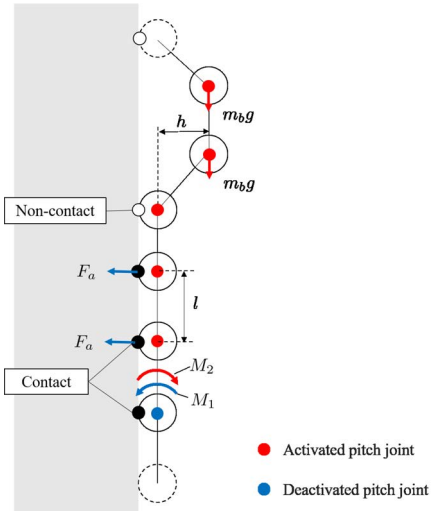

Figure 16. Moment acting on the robot when traversing a handrail.

uppermost deactivated pitch joint, there is a moment M_1 in sticking direction by the magnetic wheel and a moment M_2 in the peeling direction due to the weight of the lifting part. It is the attractive force of the magnetic wheel coaxial with the active pitch joint that affects the moment M_1. We refer to the contact point where this attraction force is generated as the effective attraction point. In order to prevent the robot from falling, $M_1 > M_2$ is required. M_1 varies depending on the number of effective attraction points determined by the range in which the pitch joints are activated. Let the attraction force be $2F_a$, the link length be l, and the number of effective attraction points be n, then M_1 can be obtained as

$$\begin{aligned} M_1 &= 2F_a l + 4F_a l + ... + 2nF_a l \\ &= 2F_a l \sum_{k=1}^{n} k \\ &= F_a l n(n+1). \end{aligned} \tag{10}$$

M_2 varies depending on the posture of the lifting unit. The center of gravity of each unit is assumed to be on the pitch axis. The moment M_2 is expected to be the largest value in the posture shown in Figure 16. Let the mass of the body unit be m_b, the acceleration of gravity be g, and the lifting height be h, then M_2 can be obtained as

$$M_2 = 2m_b g h. \tag{11}$$

The parameters (Table 2) are substituted into the equation (10)(11) to obtain $\frac{M_1}{M_2}$. When $n = 1$, $\frac{M_1}{M_2} = 6.21$, and when $n = 2$, $\frac{M_1}{M_2} = 18.6$. However, $n = 2$ is set to allow for the case where only one of the magnetic wheels is adsorbed. Similarly, $n = 2$ is set at the obstacle A where the head of the robot is lifted by the wall surface. At the obstacle B where the robot moves from the floor to the wall, where there is little possibility of flaking from the wall, $n = 1$ was set.

Figure 17. Result of the experiment of moving on a large tank at the World Robot Summit 2020.

5. Experiment

5.1. 3-D steering control

As an experiment of 3-D steering control, an experiment is conducted on a tank at the Fukushima Robot Test Field. This tank is made of steel with a radius of 2.8[m] and a height of 5[m]. A rope is attached to the robot to prevent it from falling to the ground, but tension is not generated during the experiment. The experiment started from the floor (Figure 17a). The movement from the floor to the wall (Figure 17b) is achieved by using 3-D steering control by attaching the front wheels to the wall and turning off the torque at the pitch joints. If the pitch joints are always activated, an overload error occurs at the pitch joints due to joint angle error. By deactivating the pitch joints, it is confirmed that the robot can adapt to curved surfaces. The robot is able to turn (Figure 17c) and move diagonally (Figure 17d) on the tank wall, which requires rotation in the roll direction. The robot is also able to move laterally on the tank wall, which is prone to peeling. In addition, the robot is able to move on uneven surface of the tank wall only by 3-D steering control. Therefore, it is confirmed that the developed robot could move on a curved surface by 3-D steering control with the deactivated pitch joint. Overloading of the wheel motor and yaw joint sometimes occurs during the experiment. In order to prevent the overloading, it is necessary to take into account that the magnetic wheel does not allow slippage.

For the experiment of duct inspection, the wheels are changed to non-magnetic wheels, and lights are installed at the head and tail unit. Figure 18 shows the image of the camera when the robot detects the target. The robot is able to reach the deepest part of the L-shaped duct beyond the bend. The robot is also able to detect objects and QR codes placed at various positions such as the sides and top of the duct. Even if passive roll joints are added to an articulated mobile robot, it can move in the duct without any problem. Therefore, it is confirmed that the robot has high mobility and work performance in narrow spaces.

5.2. Obstacle traversal control

Three types of obstacle traversal control are tested in laboratory experiment. A curved steel wall with a radius of 1.8 [m] and a height of 2 [m] is used for the experiment. The robot is positioned along predetermined traversing route at the start of the experiment.

The robot is able to traverse obstacle A (Figure 19) and B (Figure 20) , but is unable to traverse obstacle C (Figure 21). Figure 19, 20, 21 show the time variation of the pitch joint angle and active joints when traversing obstacles. The pitch joints are listed as pitch joint 1, 2 ,...,6 from the head of the robot. The graph background

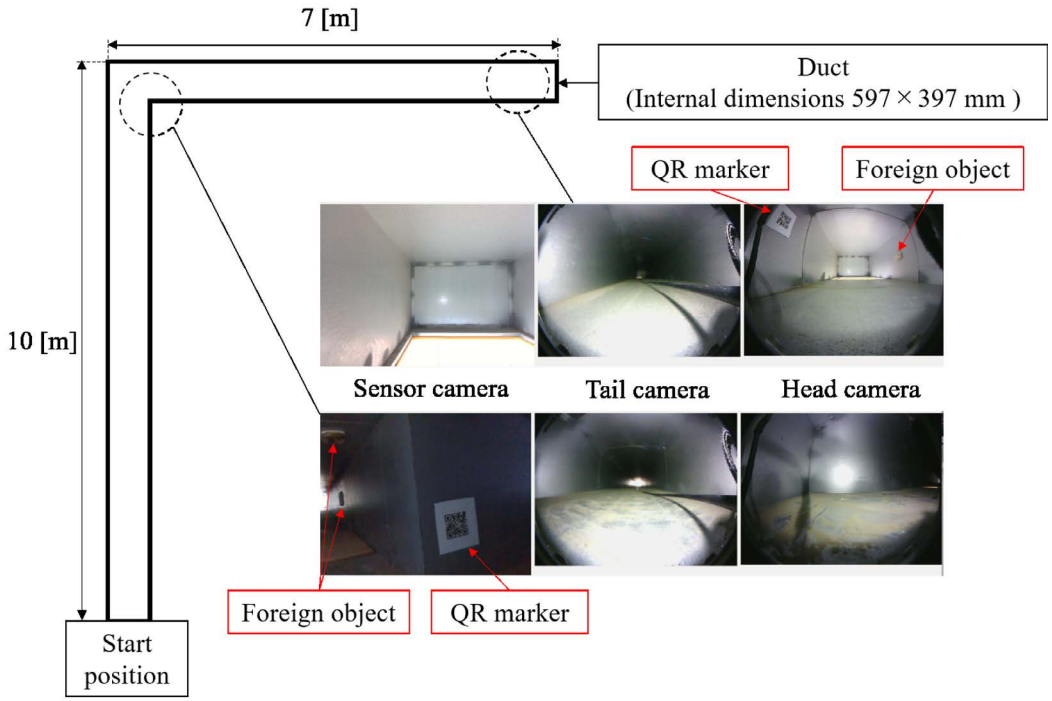

Figure 18. Result of the experiment of moving in a duct at the World Robot Summit 2020.

of the section with active joints is colored in yellow, and target values are given only for this section. The graphs show that the robot performs a lifting motion with the angle of the joints change from the leading side, and that n joints in front of the lifting motion are active. For example, pitch joint 2 and 3 are active at $t = 10$[s] in Figure 19 where pitch joint 1 starts the lifting motion at the obstacle. Therefore, the number of effective attraction points $n = 2$ are kept at the obstacle A. From the above, it is confirmed that the robot lifted its wheels and stepped over the obstacle A and B as targeted.

In contrast, Figure 22 shows the detail when the robot fail when traversing obstacle C. First, the head moves away from the wall (Figure 22a) due to the position error of the head caused by rigidity of the robot. Next, the magnetic wheels on the second unit is supposed to be lifted according to the route. However, the torque of the pitch joint is insufficient to peel the wheels off. The head of the robot approaches the wall because the pitch joint does not move as intended. At this point, the combined force in sticking direction generated on the second unit decreases due to the attraction force of the magnetic wheel and the torque of the pitch joint (Figure 22b). Then, the head of the robot collides with the wall (Figure 22c). This impact causes the second magnetic wheel to peel off abruptly, and a force is generated in the direction away from the wall (Figure 22d). The attraction force at the head unit cannot withstand this force and the robot peels off (Figure 22e). Therefore, the reasons of the robot fails to traverse obstacle C can be concluded as the positional error of the head unit, the sudden peeling of the magnetic wheels and the insufficient attraction force of the head unit. These problem must be solved in order to realize the operation of traversing obstacle C.

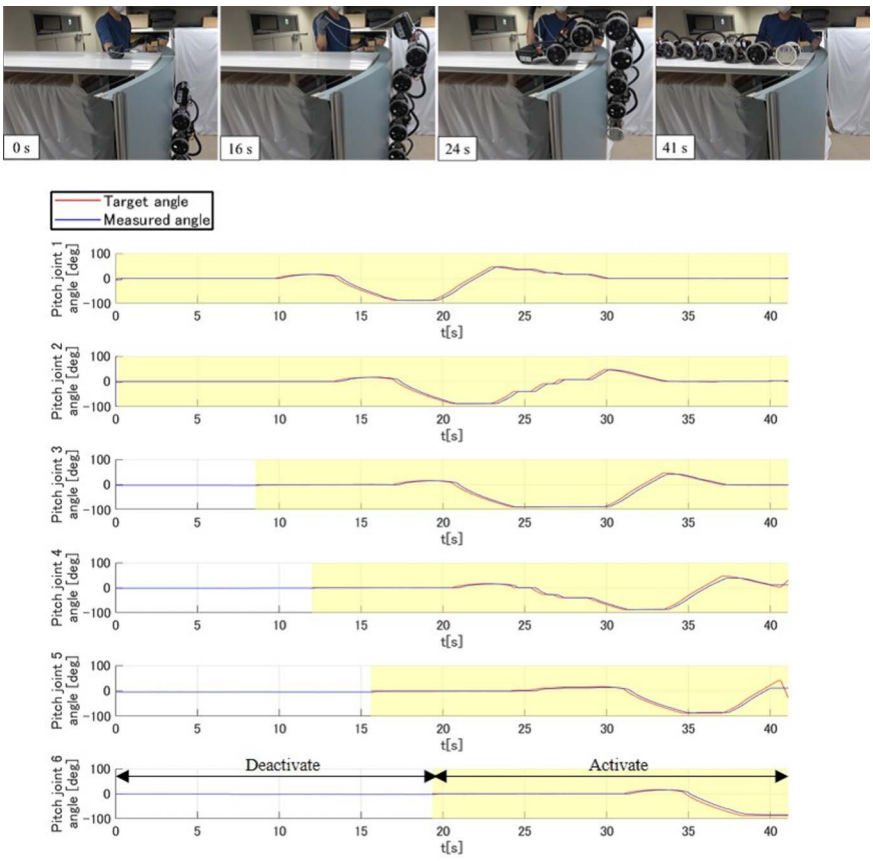

Figure 19. Result of the experiment of traversing obstacle A.

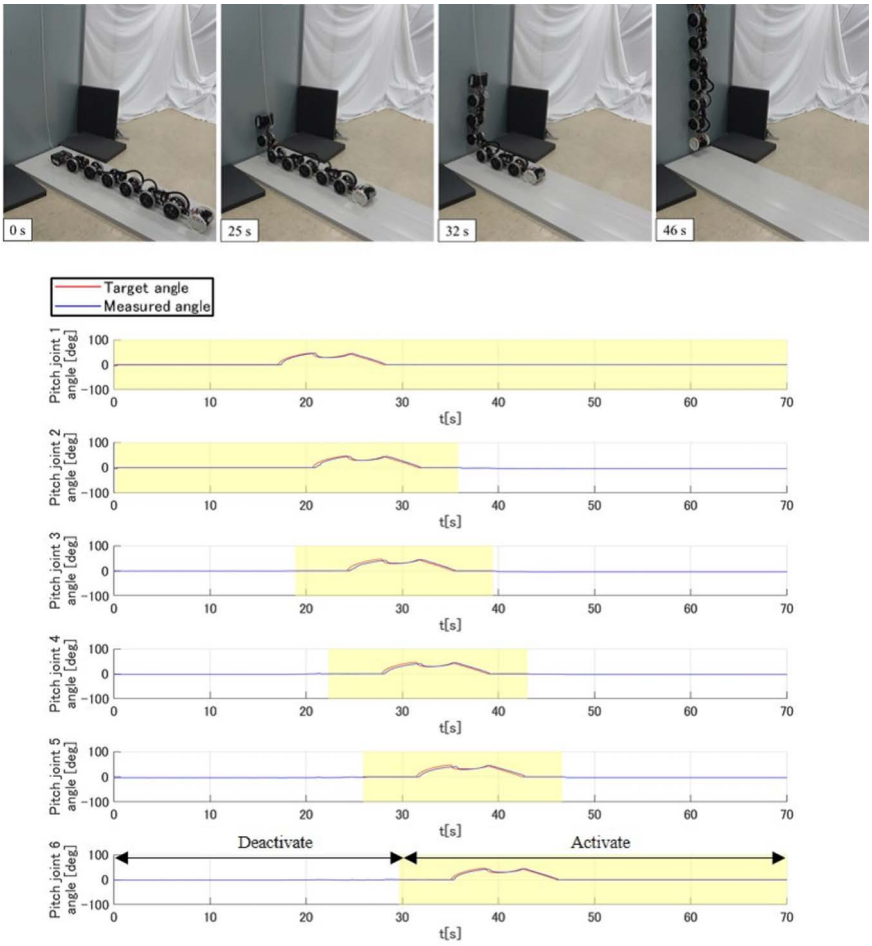

Figure 20. Result of the experiment of traversing obstacle B.

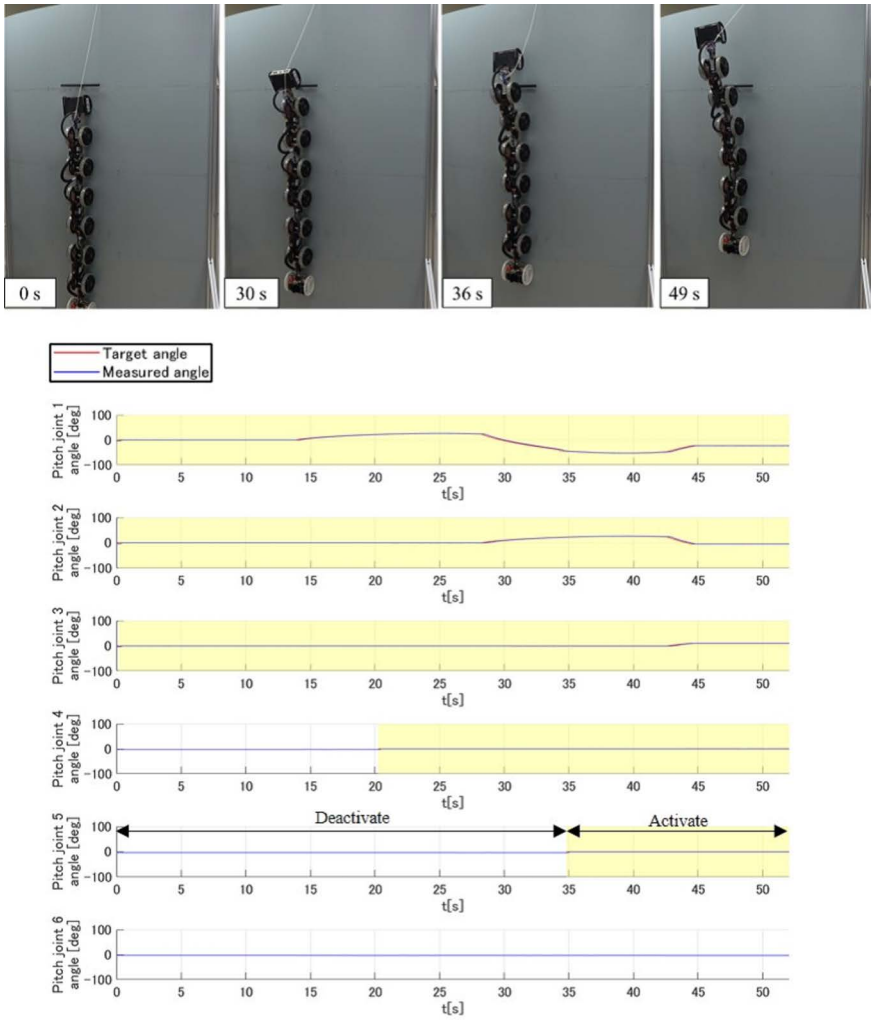

Figure 21. Result of the experiment of traversing obstacle C.

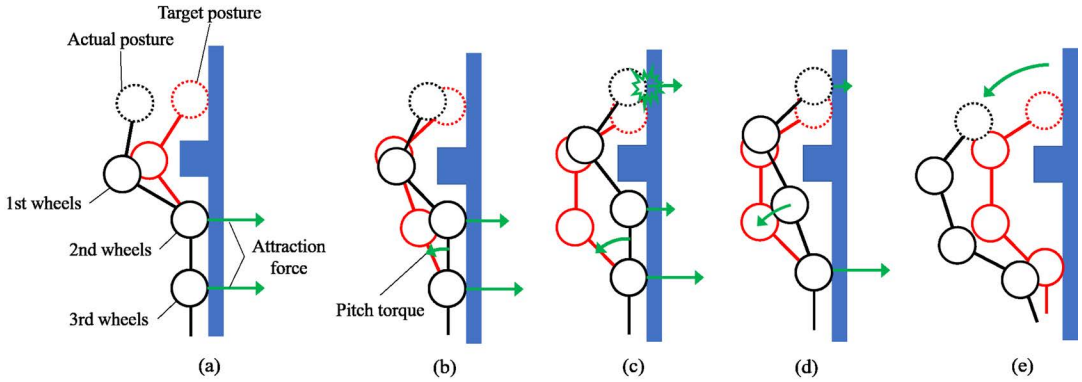

Figure 22. Flow of the robot fall at obstacle C.

6. Conclusion

In this study, we developed an articulated mobile robot that can move on the curved wall and traverse obstacles for the purpose of tank wall inspection. The developed robot is equipped with passive roll joints and magnetic wheels. The robot can adapt to the curved surface by passively rotating its roll joints and pitch joints. The robot can move on a curved wall by sticking on the wall with magnetic wheels. To ensure traverse obstacle on the wall climbing, we adjust the attraction force and friction force of the robot by designing the magnetic wheels appropriately according to the requirements and the pitch joints are locally activated. Through the experiments on the curved wall surface, we confirm that the robot can move on the tank wall and can traverse some obstacles on the corner. However, the robot cannot traverse an obstacle near the wall such as a handrail. Through the experiments in the duct, we also confirm that the robot has high mobility and work performance in narrow spaces.

The future task is to improve the obstacle traversing motion. In the traversing motion on the wall, the positional error of the head, the sudden peeling of the magnetic wheel, and the insufficient attraction force of the head greatly affect the peeling. In order to realize the obstacle traversing, we plan to improve the design of the robot and the obstacle traversing motion.

Acknowledgements

The authors would like to thank the members of our laboratory for helpful discussions and their valuable cooperation in the experiments. This work was partially supported by JSPS KAKENHI Grant Numbers JP21H01285.

References

[1] Siyuan W. Research status and future development of wall-climbing robot. International Conference on Electronics, Circuits and Information Engineering; 2021; 22-130.

[2] Han L, Wang L, Zhou J, Wang Y. The development status of ship wall-climbing robot. International Conference on Electron Device and Mechanical Engineering; 2021; 231-237.

[3] Zhiqi R. Design and Research of Negative Pressure Adsorption Wall-Climbing Robots. North China Electric Power University; 2018; 201-8.

[4] Dedong T. Research on Negative Pressure Adsorption Wall-Climbing Robots and Control. Beijing Institute of Technology; 2016; 13-3: 201-211.

[5] Shigui X, Ya ' nan Z, Linyong S, Wei S, Jinwu Q. Research on a Twin-body Negative Pressure Wall-climbing Robot. Industrial Control Computer; 2018; 31-06: 85-87.

[6] Eich M, Vogele T. Design and Control of a Lightweight Magnetic Climbing Robot for Vessel Inspection. 2011 19th Mediterranean Conference on Control & Automation (MED); 2011; 1200-1205.

[7] Eiammanussakul T, Taoprayoon J, Sangveraphunsiri V. Weld Bead Tracking Control of a Magnetic Wheel Wall Climbing Robot Using a Laser-Vision System. Applied Mechanics and Materials;2014. 219-223.

[8] Fernández R, González E, Feliú V, Rodríguez AG. A wall climbing robot for tank inspection. An autonomous prototype. IECON 2010 - 36th Annual Conference on IEEE Industrial Electronics Society; 2010; 1424-1429.

[9] Leon-Rodriguez H, Hussain S, Sattar T. A compact wall-climbing and surface adaptation robot for non- destructive testing. 2012 12th International Conference on Control, Automation and Systems; 2012; 404-409.

[10] Burmeister A, Pezeshkian N, Talke K, Ostovari S, Everett HR, Hart A, Gilbreath G, Nguyen HG. Design of a Multi-Segmented Magnetic Robot for Hull Inspection. ASNE Mega Rust 2014: Naval Corrosion Conference, San Diego, CA; 2014 June 24-26.
[11] Lee G, Seo K, Lee S, Park J, Kim H, Kim J, Seo T. Compliant track-wheeled climbing robot with transitioning ability and high-payload capacity. 2011 IEEE International Conference on Robotics and Biomimetics;2011; 2020-2024.
[12] Lee G, Wu G, Kim SH, Kim J, Seo T. Combot: Compliant climbing robotic platform with transitioning capability and payload capacity. 2012 IEEE International Conference on Robotics and Automation;2012; 2737- 2742.
[13] Wang H, Huang X, Hong R, Fang C. A new inspection robot system for storage tank. 008 7th World Congress on Intelligent Control and Automation; 2008; 7427-7431.
[14] Liu J, Xu L, Chen S, Xu H, Cheng G, Xu J. Development of a bio-inspired wall-climbing robot composed of spine wheels, adhesive belts and eddy suction cup. Robotica; 2021; 39-1: 3-22.
[15] Yanwei L, Limeng W, Sanwa L, Tao M, Pengyang L, Yan L. Design and Analysis of an Inchworm-Inspired Wall-Climbing Robot. Journal of Mechanical Transmission; 2019; 43-08: 87-91.
[16] Fabien T, Wolfgang F, Gilles C, Roland S. Magnebike: A Magnetic Wheeled Robot with High Mobility for Inspecting Complex-Shaped Structures. Journal of Field Robotics; 2009; 26-5: 453-476.
[17] Tanaka M, Nakajima M, Suzuki Y, Tanaka K. Development and Control of Articulated Mobile Robot for Climbing Steep Stairs. IEEE/ASME Transactions on Mechatronics; 2018; 23-2: 531-541.
[18] Fjerdingen SA, Liljebäck P, Transeth AA. A snake-like robot for internal inspection of complex pipe structures (PIKo). 2009 IEEE/RSJ International Conference on Intelligent Robots and Systems; 2009; 5665-5671.
[19] Yamada H, Hirose S. Development of Practical 3-Dimensional Active Cord Mechanism ACM-R4. Journal of Robotics and Mechatronics; 2006; 18-3: 305-311.
[20] Yamada H, Takaoka S, Hirose S. A snake-like robot for real-world inspection applications (the design and control of a practical active cord mechanism). Advanced Robotics; 2013; 27-1: 47-60.
[21] Kouno K, Yamada H, Hirose S. Development of Active-Joint Active-Wheel High Traversability Snake-Like Robot ACM-R4.2. Journal of Robotics and Mechatronics; 2013; 25-3: 559-566.
[22] Tanaka M, Nakajima M, Tanaka K. Smooth control of an articulated mobile robot with switching constraints. Advanced Robotics; 2016; 30-1: 29-40.
[23] Tanaka M, Tadakuma K, Nakajima M, Fujita M. Task-Space Control of Articulated Mobile Robots With a Soft Gripper for Operations. IEEE Transactions on Robotics; 2018; 35-1, 135-146.
[24] Daltorio KA, Horchler AD, Gorb S, Ritzmann RE ,Quinn RD. A small wall-walking robot with compliant, adhesive feet. 2005 IEEE/RSJ International Conference on Intelligent Robots and Systems; 2005; 3648-3653.
[25] Zhiwei X, Muhua C, Qingji G. The structure and defects recognition algorithm of an aircraft surface defects inspection robot. 2009 International Conference on Information and Automation; 2009; 740-745.
[26] Wu S, Wu L, Liu T. Design of a sliding wall climbing robot with a novel negative adsorption device. 2011 8th International Conference on Ubiquitous Robots and Ambient Intelligence (URAI); 2011; 97-100.
[27] Silva MF, Barbosa RS, Oliveira ALC. Climbing Robot for Ferromagnetic Surfaces with Dynamic Adjustment of the Adhesion System. Hindawi Publishing Corporation Journal of Robotics; 2012.
[28] Yamada H, Hirose S. Study of Active Cord Mechanism -Approximations to Continuous Curves of Multi-joint Body-. Journal of the Robotics Society of Japan; 2008; 26-1: 110-120.